Colloquia: LaThuile14

Testing the new physics scale in the B^0 system at ATLAS

C. Alpigiani on behalf of the ATLAS Collaboration

School of Physics and Astronomy, Queen Mary University of London
Mile End Road E1 4NS - London, UK

Summary. — Weak decays that are naturally suppressed in the Standard Model (SM), such as processes with flavour-changing neutral currents, are perfect for indirect searches of new physics. These decays allow us to investigate higher energy ranges with respect to direct searches thus representing a fundamental complementary tool. Results on the ATLAS analysis of the $B_s^0 \to \mu^+\mu^-$ rare decay will be presented. The ATLAS study of $B_d^0 \to K^{*0}\mu^+\mu^-$ is also reported where the parameters A_{FB} and F_L are extracted from the angular distribution of the final state. The measurement of the ϕ_s phase in the $B_s^0 \to J/\psi\,\phi$ system, that can provide probes for physics beyond the SM, is showed too.

PACS `13.20.He` – Decays of bottom mesons.

1. – Introduction

ATLAS (A Toroidal Lhc ApparatuS) is a general purpose experiment [1] operating at the Large Hadron Collider (LHC) at CERN. ATLAS can perform high-quality measurements of CP-violating phase in the $B_s^0 \to J/\psi\,\phi$ decay and indirect searches for new physics such as rare decay $B_s^0 \to \mu^+\mu^-$ and $B_d^0 \to K^{*0}\mu^+\mu^-$. These are complementary tools to direct searches for new physics and can provide precise measurements to compare with SM predictions and set important constraints to new physics model building.

In this document, the results of analyses of the above decays on $4.9\,\mathrm{fb}^{-1}$ of data collected by the ATLAS detector in 2011 are presented.

2. – $B_s^0 \to \mu^+\mu^-$

The rare decay $B_s^0 \to \mu^+\mu^-$ is highly suppressed in the SM and can only occur via higher-order diagrams. The expected SM branching ratio is $(3.27 \pm 0.27) \cdot 10^{-9}$ [2] and both CMS and LHCb Collaborations showed evidence in this channel with a measured BR of $(2.9 \pm 0.7) \cdot 10^{-9}$ [3,4].

2˙1. *Analysis strategy.* – The analysis of the rare B_s^0 decay [5] is based on events selected by the di-muon trigger and reconstructed in the inner detector and the muon spectrometer. The method adopted is based on a "cut & count" approach that uses a Multi-Variate Analysis (MVA) in order to discriminate between signal and background events.

The branching ratio is studied relative to a similar (well known) SM branching ratio with a sufficient observed statistics. This allows to reduce the production and efficiency uncertainties that mostly cancel out in the ratio.

In order to avoid biases in the final results, a blind analysis is performed: all data in the invariant mass region $[5066, 5666]$ MeV are removed from the analysis until the procedure for the events selection, optimisation and limit extraction is completely defined and agreed upon.

Relative to the well known channel $B^+ \to J/\psi(\to \mu^+\mu^-)K^+$, the $B_s^0 \to \mu^+\mu^-$ branching ratio can be expressed as

$$(1) \qquad \mathrm{BR}(B_s^0 \to \mu^+\mu^-) = \mathrm{BR}(B^+ \to J/\psi\,K^+)\frac{\varepsilon_{J/\psi\,K^+} \cdot A_{J/\psi\,K^+}}{\varepsilon_{\mu\mu} \cdot A_{\mu\mu}} \cdot \frac{f_u}{f_s} \cdot \frac{N_{\mu\mu}}{N_{J/\psi\,K^+}},$$

$$(2) \qquad \mathrm{SES} = \mathrm{BR}(B^+ \to J/\psi\,K^+)\frac{\varepsilon_{J/\psi\,K^+} \cdot A_{J/\psi\,K^+}}{\varepsilon_{\mu\mu} \cdot A_{\mu\mu}} \cdot \frac{f_u}{f_s} \cdot \frac{1}{N_{J/\psi\,K^+}},$$

where, for each mode, N is the number of observed events, ε and A are the absolute efficiencies and acceptances, respectively, and f_u/f_s is the relative production rate of B^+ and B_s^0 in pp collisions.

The $B_s^0 \to \mu^+\mu^-$ event selection is made up of a baseline set of cuts followed by final selection based on a Boosted Decision Tree (BDT) and optimised on half of the sideband data. The number of signal events can be estimated from the number of observed events in the signal region and the number of expected background events in the same region, where the background is interpolated from the still-unused half of sideband sample.

The limit on $N_{\mu\mu}$ reflects into a limit on $\mathrm{BR}(B_s^0 \to \mu^+\mu^-)$ through a multiplicative coefficient referred to as Single Event Sensitivity (SES). The uncertainty on the SES itself is non-negligible and needs to be taken into account in the determination of the upper-limit on $\mathrm{BR}(B_s^0 \to \mu^+\mu^-)$, effectively treating the SES as an efficiency correction (with uncertainty) to the event yield.

The terms $\varepsilon \cdot A$ are obtained from the Monte Carlo with systematic uncertainties estimated from the residual data-MC discrepancies observed in the $B^+ \to J/\psi\,K^+$ control sample, while the B^+ yield is obtained with an un-binned maximum-likelihood fit after having applied a selection similar to that applied to the signal channel in order to minimise the systematic uncertainties in the ratio.

The B^+ experimental branching ratio is taken from the PDG [6], whereas, regarding the ratio f_u/f_s, the last LHCb measurement is considered [7].

The expected background in the signal region can be essentially subdivided in two categories: a continuum background and resonant component. The continuum contribution has a smooth dependence on the di-muon invariant mass and can be rejected by studying the event topology. Figure 1 shows two of the most discriminating variables used in the analysis. The resonant background peaks into the signal region and is composed by $B \to hh$ events ($h = K^{\pm}$ or $\pi^{\pm}$) in which the hadrons are misidentified as muons. The resonant background contribution is estimated using MC and included in both the optimisation procedure and the evaluation of the expected background yield for the upper limit extraction.

2˙2. *Results on* $4.9\,\mathrm{fb}^{-1}$. – The upper limit on the $B_s^0 \to \mu^+\mu^-$ branching ratio is extracted following the ATLAS prescription for the extraction of the frequentist limits by

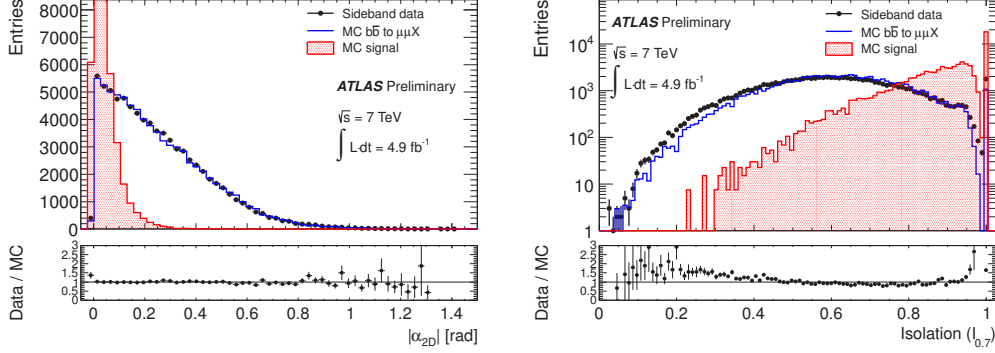Fig. 1. – Comparisons between sideband data (black dots) and data-reweighted $b\bar{b} \to \mu^+\mu^- X$ MC events (blue solid histogram) for two of the most powerful separation variables. $|\alpha_{2D}|$ (left) is the angle in the transverse plane between the vector from the primary vertex to the B decay vertex and the momentum of the B. $I_{0.7}$ (right) is the B isolation, defined as the ratio of $|\vec{p}_T^B|$ to the sum of $|\vec{p}_T^B|$ and the transverse momenta of all tracks with $p_T > 0.5\,\mathrm{GeV}$ within a cone $\Delta R < 0.7$ from the B direction, excluding the B decay products. The signal (red-filled solid histogram) is shown for shape comparison. Uncertainties are statistical only. The lower graph in each case shows the data/MC ratio.

means of the standard implementation [8,9] of the CL_s method [10]. Table I summarises all the inputs necessary for the evaluation of the $B_s^0 \to \mu^+\mu^-$ branching ratio.

Before the un-blinding, the median of the expected upper limit is obtained, setting the count in the signal region (N_{SR}^{obs}) equal to the background interpolated from the sidebands plus the small contribution from the resonant background (N_{SR}^{exp}), to be $1.6 \cdot 10^{-8}$ ($1.3 \cdot 10^{-8}$) at 95% CL (90% CL).

After the un-blinding, 6 events have been observed in the signal region (N_{SR}^{obs}) giving an observed upper limit $\mathrm{BR}(B_s^0 \to \mu^+\mu^-) < 1.5\,(1.2) \cdot 10^{-8}$ at 95% (90%) CL. Figure 2 shows the distribution of the observed $\mu^+\mu^-$ candidates and the CL_s behaviour for different signal strength evaluated using 300000 toy Monte Carlo simulations per point.

TABLE I. – *Input values used for the extraction of the upper limit using the CL_s method. The first two rows show the B^+ yield $N_{J/\psi K^\pm}$ and the ratio of the acceptance times selection efficiency for the B_s^0 signal and the B^+ reference channel, $R_{A\varepsilon}$, used in the evaluation of the SES.*

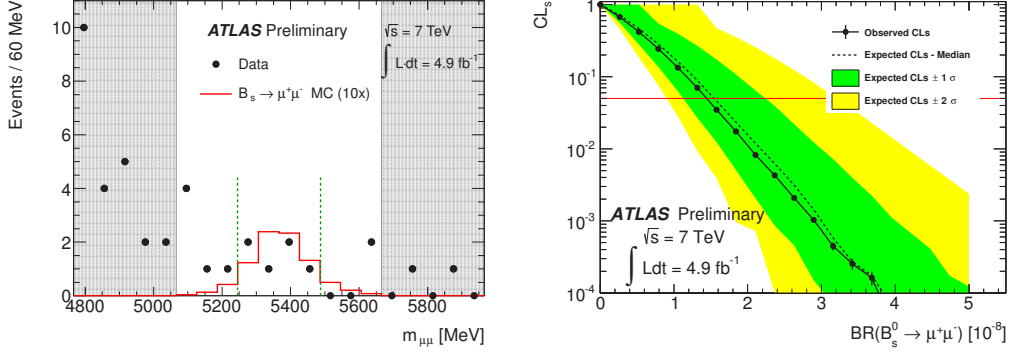| Quantity	Value
$N_{J/\psi K^\pm}$	$15214 \pm 1.10\% \pm 2.39\%$
$R_{A\varepsilon}$	$0.267 \pm 1.8\% \pm 6.9\%$
SES	$(2.07 \pm 0.26) \cdot 10^{-9}$
R_{bkg}^{obs}	1.240 ± 0.050
$N_{SR}^{exp} \mid N_{SR}^{obs}$	$6.75 \mid 6$
$N_{bkg,SB}^{obs}$	8
$N_{B \to hh}$	0.30

Fig. 2. – Left: Invariant-mass distribution of selected candidates in data (dots). The plot also indicates the signal (continuous line) as predicted by Monte Carlo assuming BR($B_s^0 \to \mu^+\mu^-$) = $3.5 \cdot 10^{-8}$ (increased by a factor 10), the optimised signal window (two dashed vertical lines) and the sidebands used in the analysis (grey areas). The expected number of $B_s^0 \to \mu^+\mu^-$ signal in the signal region is 1.7 ± 0.2 events. The expected background yield per bin in the signal region is 1.7 events. Right: Observed CL_s (circles) as a function of BR($B_s^0 \to \mu^+\mu^-$). The 95% CL limit is indicated by the horizontal (red) line. The dark (green) and light (yellow) bands correspond to the $\pm 1\,\sigma$ and $\pm 2\,\sigma$ ranges of the background-only pseudo-experiments with the median of the expected CL_s given by the dashed line.

3. $- B_d^0 \to K^{*0}\mu^+\mu^-$

In the SM, the $B_d^0 \to K^{*0}(\to K^+\pi^-)\mu^+\mu^-$ decay occurs via loop diagrams that mediate the transition $b \to s\,l^+l^-$ and therefore has a small branching ratio of $(1.06 \pm 0.1) \cdot 10^{-6}$. The angular distribution of the 4 final-state particles and the decay amplitudes are sensitive to new physics due to interference with SM diagrams.

3˙1. *Angular analysis*. – The $B_d^0 \to K^{*0}\mu^+\mu^-$ decay [11] is described by four kinematic variables, one being the invariant mass q^2 of the di-muon system and the other three being angles describing the geometrical configurationf of the final state depicted in fig. 3. θ_L is the angle between the μ^+ and the direction opposite to the B_d^0 in the di-muon rest frame, θ_K is the angle between the K^+ and the direction opposite to the B_d^0 in the K^{*0} rest frame, and ϕ is the angle between the plane defined by the two muons and the plane defined by the kaon-pion system in the B_d^0 rest frame.
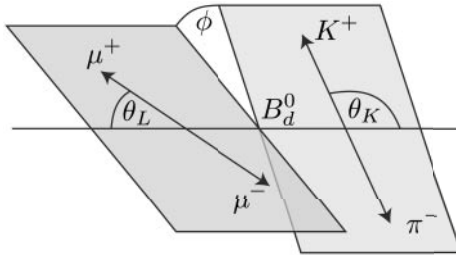

Fig. 3. – Definition of the kinematic angles in the $B_d^0 \to K^{*0}\mu^+\mu^-$ decay.

Since the statistics available in 2011 is not sufficient to allow a complete 3D angular analysis, the differential decay rate is projected into the 2-dimensional distributions (showed in the following eqs. (3) and (4)) obtained by integrating over the two other variables:

(3)
$$\frac{1}{\Gamma}\frac{\mathrm{d}^2\Gamma}{\mathrm{d}q^2\,\mathrm{d}\cos\theta_L} = \frac{3}{4}F_L\left(q^2\right)\left(1-\cos^2\theta_L\right)$$

$$+\frac{3}{8}\left(1-F_L\left(q^2\right)\right)\left(1+\cos^2\theta_L\right)+A_{FB}\left(q^2\right)\cos\theta_L,$$

(4)
$$\frac{1}{\Gamma}\frac{\mathrm{d}^2\Gamma}{\mathrm{d}q^2\,\mathrm{d}\cos\theta_K} = \frac{3}{2}F_L\left(q^2\right)\cos^2\theta_K + \frac{3}{4}\left(1-F_L\left(q^2\right)\right)\left(1-\cos^2\theta_K\right),$$

F_L is the fraction of longitudinal polarisation and A_{FB} is the muon forward-backward asymmetry extracted binning the distributions in intervals of q^2 that coincide with those used in the Belle analysis [12].

The main sources of background are coming from $b\bar{b} \to \mu^+\mu^- X$ combinatorial events with small contributions from $c\bar{c} \to \mu^+\mu^- X$ and Drell-Yan, and resonant contribution from different exclusive decay channels.

To increase the analysis sensitivity in the F_L and A_{FB} measurements, the final selection cuts are optimised maximising the estimator $N_{sig}/\sqrt{N_{sig}+N_{bkg}}$, where N_{sig} is the number of selected signal events and N_{bkg} the number of background events. Additional cuts are introduced to remove the radiative charmonium decays $B_d^0 \to K^{*0}J/\psi$ (with $J/\psi \to \gamma\mu^+\mu^-$) and $B_d^0 \to K^{*0}\psi(2S)$ (with $\psi(2S) \to \gamma\mu^+\mu^-$), and to remove the tails from J/ψ and $\psi(2S)$ reconstruction.

Due to the small available statistics in the low di-muon invariant mass region, the F_L and A_{FB} parameters are extracted by means of a sequential unbinned maximum-likelihood fit that provides a more stable fitting procedure. Firstly the invariant mass distribution $K\pi\mu\mu$ is fitted (modelling the signal with a Gaussian and the background with an exponential) and the resulting parameters are fixed, then the angular distributions are fitted fixing the signal and background yields from the previous fit. Tests performed comparing the above procedure with the simultaneous fit strategy show that the sequential fit does not introduce significant bias in the analysis and the errors of the fit parameters are the same for both cases.

3.2. *Results on* 4.9 fb^{-1}. – The final results of the un-binned maximum-likelihood fit are reported in fig. 4 for F_L and A_{FB} compared to the SM expectations. The theoretical expectations have been calculated for the limit of large q^2 [13] and small q^2 [14] (no expectation is given for the central q^2 region). The results obtained on 4.9 fb^{-1} of data are mostly consistent with the SM predictions, but the measurement is still statistically limited.

4. – $B_s^0 \to J/\psi\,\phi$

The B_s^0 system can provide excellent probes to test new physics in the CP violation since new phenomena beyond the SM may enter in the loop-mediated B_s^0 mixing process and lead to discrepancies with the SM expectations. The time evolution of B_s^0 meson mixing is characterised by the mass difference Δm_s of the heavy B_H and light B_L mass
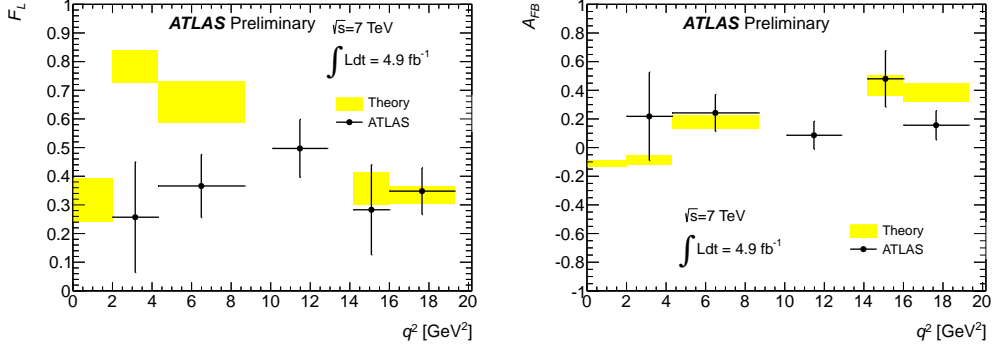
Fig. 4. – Fraction of longitudinal polarisation F_L (left) and muons forward-backward asymmetry A_{FB} (right) measured by ATLAS on $4.9\,\mathrm{fb}^{-1}$ of data collected in 2011 compared with the theoretical prediction evaluated for the limit of small and large q^2 values including the related uncertainties [15].

eigenstates, the CP-violating mixing phase ϕ_s and the width difference $\Delta\Gamma_s = \Gamma_L - \Gamma_H$ of B_L and B_H .

In the SM, the phase ϕ_s is small and can be related to CKM quark mixing matrix elements via the relation $\phi_s \simeq -2\beta_s = -2\arg[-(V_{ts}V_{tb}^*)/(V_{cs}V_{cb}^*)] = -0.0368\pm0.0018\,\mathrm{rad}$ measured via global fits to experimental data [16]. However, the small uncertainty makes the direct measurement interesting since new physics could modify the phase ϕ_s if new particles enter the B_s-$\overline{B}_s$ box diagrams. Physics beyond the SM is not expected to affect $\Delta\Gamma_s$ as significantly as ϕ_s. Nevertheless, the measurement of $\Delta\Gamma_s$ is useful as it allows theoretical predictions to be tested.

We present here the ATLAS measurements of ϕ_s, the average decay width $\Gamma_s = (\Gamma_L + \Gamma_H)/2$ and $\Delta\Gamma_s$ using the flavour-tagged time-dependent analysis on $4.9\,\mathrm{fb}^{-1}$ of data collected in 2011 [17].

4˙1. *Angular analysis.* – The $B_s^0 \to J/\psi\,\phi$ final state is an admixture of different CP eigenstates (CP-odd and CP-even states with orbital angular momentum $L = 0$, 1 or 2). In order to disentangle them, the time-dependent angular distribution of the final-state particles, described by eq. (5) (for more details see [18]), has to be performed.

$$
(5) \qquad f(t, \theta_T, \psi_T, \phi_T) = \sum_{k=1}^{10} \mathcal{O}^{(k)}(t) \cdot g^{(k)}(\theta_T, \psi_T, \phi_T).
$$

The functions $\mathcal{O}^{(k)}(t)$ describe the evolution of the angular distributions with the proper time of the B_s^0 decay and are expressed in term of the linear polarisation amplitudes $A_0(t)$, $A_\parallel(t)$ and $A_\perp(t)$, while $g^{(k)}$ are the 10 angular functions. Flavour tagging is used to distinguish between the initial B_s^0 and $\overline{B}_s^0$ states.

Figure 5 illustrates the angles used in the analysis that are defined in the rest frame of the final-state particles. The x axis is determined by the direction of the ϕ meson in the
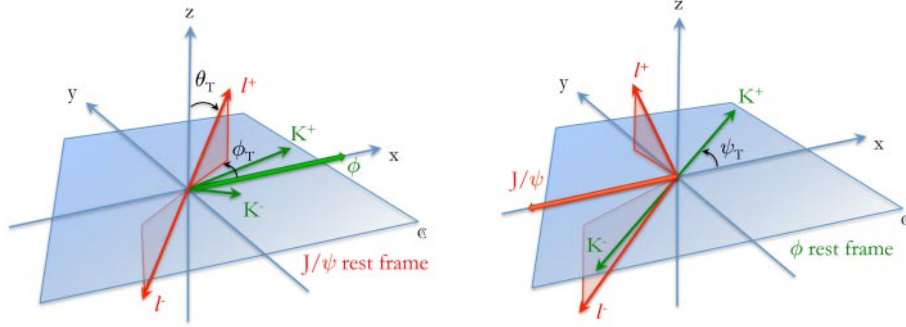
Fig. 5. – Schematic definition of coordinate systems and angles for the $B_s^0 \rightarrow J/\psi\,\phi$ decay.

J/ψ rest frame while the K^+K^- plane defines the xy-plane. θ_T is the angle between μ^+ momentum $p(\mu^+)$ and the xy-plane in the J/ψ meson rest frame, ϕ_T is the angle between the x-axis and the projection of the μ^+ momentum in the xy-plane $p_{xy}(\mu^+)$ in the J/ψ rest frame, finally ψ_T is the angle between $p(K^+)$ and $-p(J/\psi)$ in the ϕ meson rest frame.

4‘2. *Flavour tagging.* – The determination of the initial flavour of the neutral B meson can be inferred using the information from the other B meson that is typically produced from the other b quark in the event, referred as the Opposite-Side Tagging (OST). This method has been studied and calibrated on $B^\pm \rightarrow J/\psi K^\pm$ samples in which the flavour of the charge of the B meson at production is given by the charge of the kaon.

Two different tagging methods are used in the analysis, a *muon tagger* in which the charge is identified through the semi-leptonic decay of the B and a *charge jet tagger* [19] that considers tracks associated to the jet from the same primary vertex of the signal decay. The two methods are combined according to the hierarchy of performances. If it is not possible to provide a tagging response for the event, the tagging probability is set to 0.5.

4‘3. *Results on* $4.9\,\text{fb}^{-1}$. – An un-binned maximum-likelihood fit including a tagging probability is performed to extrapolate the signal and the fitted values of the physical parameters obtained on $4.9\,\text{fb}^{-1}$ of data are reported in table II.

TABLE II. – *Fitted values for the physical parameters along with their statistical and systematic uncertainties.*

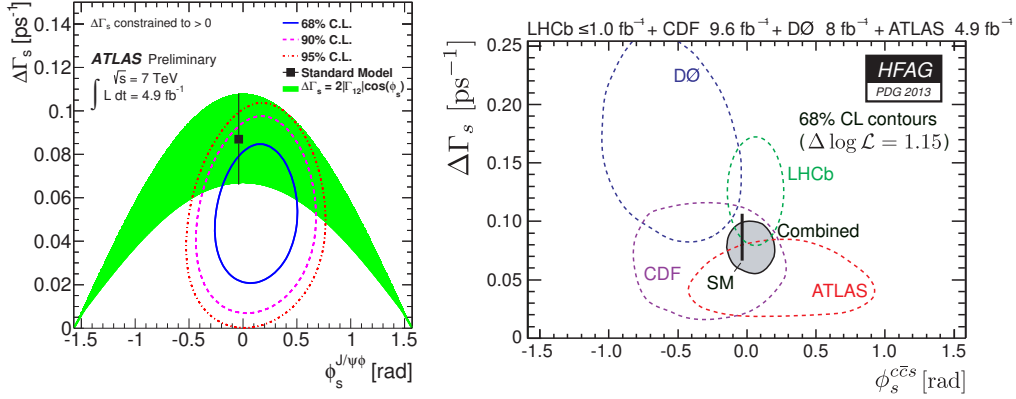| Parameter	Value	Statistical uncertainty	Systematic uncertainty
ϕ_s (rad)	0.12	0.25	0.11
$\Delta\Gamma_s$ (ps^{-1})	0.053	0.021	0.009
Γ_s (ps^{-1})	0.677	0.007	0.003
$|A_\parallel(0)|^2$	0.220	0.008	0.009
$|A_0(0)|^2$	0.529	0.006	0.011
$|A_S|^2$	0.024	0.014	0.028
$\delta_\perp$	3.89	0.46	0.13

Fig. 6. – Left: likelihood contours in ϕ_s-$\Delta\Gamma_s$ plane. The blue and red lines show the likelihood contours for 68% and 95% confidence intervals, respectively (statistical errors only). The green band is the theoretical prediction of mixing-induced CP violation. Right: HFAG comparison and combination of the ATLAS results with the results of other experiments [20].

Figure 6 reports the obtained likelihood contours in the ϕ_s-$\Delta\Gamma_s$ plane as well as the comparison and the combination of the ATLAS results with the results obtained by other experiments [20]. All the results are in good agreement with the SM expectations.

REFERENCES

[1] ATLAS COLLABORATION, *JINST*, **3** (2008) S08003.
[2] BURAS *et al.*, *Eur. Phys. J. C*, **72** (2012) 2172.
[3] CMS COLLABORATION, *Phys. Rev. Lett.*, **111** (2013) 101804.
[4] AAIJ R. *et al.* (LHCb COLLABORATION), *Phys. Rev. Lett.*, **111** (2013) 101805.
[5] ATLAS COLLABORATION, ATLAS-CONF-2013-076,
    http://cds.cern.ch/record/1562934.
[6] BERINGER J. *et al.* (PARTICLE DATA GROUP), *Phys. Rev. D*, **86** (2012) 010001.
[7] AAIJ R. *et al.* (LHCb COLLABORATION), *JHEP*, **04** (2013) 001.
[8] BRUN R., CANAL P. and RADEMAKERS F., *PoS ACAT*, **2010** (2010) 002.
[9] JUNK T., *Nucl. Instrum. Methods A*, **434** (1999) 435.
[10] READ A. L., *J. Phys. G*, **28** (2002) 2693.
[11] ATLAS COLLABORATION, ATLAS-CONF-2013-038,
    https://cds.cern.ch/record/1537961.
[12] HARA K. *et al.* (BELLE COLLABORATION), *Phys. Rev. Lett.*, **103** (2009) 171801.
[13] BOBETH C., HILLER G. and VAN DYK D., *Phys. Rev. D*, **87** (2012) 034016.
[14] KRUGER F. and MATIAS J., *Phys. Rev. D*, **71** (2005) 094009.
[15] BOBETH C., HILLER G. and VAN DYK D., *DO-TH*, **11/02** (2011) arXiv:1105.2659.
[16] BONA M. *et al.* (UTFIT COLLABORATION), *Phys. Rev. Lett.*, **97** (2006) 151803.
[17] ATLAS COLLABORATION, ATLAS-CONF-2013-039,
    http://cds.cern.ch/record/1541823.
[18] BALL P. *et al.*, CERN-TH/2000-101, arXiv:hep-ph/0003238.
[19] ATLAS COLLABORATION, arXiv:0901.0512.
[20] AMHIS Y. *et al.* (HEAVY FLAVOUR AVERAGING GROUP (HFAG)),
    http://www.slac.stanford.edu/xorg/hfag/osc.